

## IMPORTANCE OF GIANT IMPACT EJECTA FOR ORBITS OF PLANETS FORMED DURING THE GIANT IMPACT ERA

HIROSHI KOBAYASHI, KAZUHIDE ISOYA, AND YUTARO SATO  
Department of Physics, Nagoya University, Nagoya, Aichi 464-8602, Japan  
*Draft version February 5, 2022*

## ABSTRACT

Terrestrial planets are believed to be formed via giant impacts of Mars-sized protoplanets. Planets formed via giant impacts have highly eccentric orbits. A swarm of planetesimals around the planets may lead to eccentricity damping for the planets via the equipartition of random energies (dynamical friction). However, dynamical friction increases eccentricities of planetesimals, resulting in high velocity collisions between planetesimals. The collisional cascade grinds planetesimals to dust until dust grains are blown out due to radiation pressure. Therefore, the total mass of planetesimals decreases due to collisional fragmentation, which weakens dynamical friction. We investigate the orbital evolution of protoplanets in a planetesimal disk, taking into account collisional fragmentation of planetesimals. For 100 km-sized or smaller planetesimals, dynamical friction is insignificant for eccentricity damping of planets because of collisional fragmentation. On the other hand, giant impacts eject collisional fragments. Although the total mass of giant impact ejecta is 0.1-0.3 Earth masses, the largest impact ejecta are  $\sim 1,000$  km in size. We also investigate the orbital evolution of single planets with initial eccentricities 0.1 in a swarm of such giant impact ejecta. Although the total mass of giant impact ejecta decreases by a factor of 3 in 30 Myrs, eccentricities of planets are damped down to the Earth level ( $\sim 0.01$ ) due to interaction with giant impact ejecta. Therefore, giant impact ejecta play an important role for determination of terrestrial planet orbits.

*Keywords:* Planet formation (1241), Solar system formation (1530), Inner planets (797)

## 1. INTRODUCTION

In the standard scenario for terrestrial planet formation, Mars-sized protoplanets are formed prior to the gas depletion of the protoplanetary disk (in several Myrs) with large orbital separations  $\sim 10$  mutual Hill radii (e.g., Kobayashi & Dauphas 2013). The gas depletion triggers the long term orbital instability of protoplanets and the collisions between protoplanets induced by the orbital instability result in the formation of Earth or Venus sized planets, which is called the giant impact stage (Chambers, & Wetherill 1998; Iwasaki et al. 2001).

Most of the masses of the terrestrial planets in the Solar System is in Earth and Venus, which have low eccentricities of 0.017 and 0.007, respectively. The largest planets formed in orbital simulations for giant impact stages have much greater eccentricities and inclinations than those of Earth or Venus (Chambers 2001; Kokubo et al. 2006). Those eccentricities and inclinations are possible to be damped via the equipartition of random energies (dynamical friction) with surrounding planetesimals (O'Brien et al. 2006; Raymond et al. 2009; Morishima et al. 2010). However, the surface density of surrounding planetesimals decreases via the collisional cascade of the planetesimals (Kobayashi & Tanaka 2010), which reduces the efficiency of dynamical friction. Therefore, collisional fragmentation plays an important role in this issue.

On the other hand, a series of giant impacts eject fragments with a total mass comparable to Earth, resulting in the increase of infrared emission. Therefore, giant impact ejecta explain infrared excesses caused by warm debris disks around 1 AU (Genda et al. 2015), while cold debris disks beyond 10 AU may be related to col-

lisional fragmentation in planetesimal disks induced by planet formation (Kobayashi, & Löhne 2014). Such giant-impact-ejecta disks may affect the orbital evolution of protoplanets. The evolution of total masses of giant impact ejecta is controlled by the collisional cascade. Therefore, we need to consider the orbital evolution and the collisional cascade simultaneously.

The orbital evolution of protoplanets in the giant impact stage is mainly treated by  $N$ -body simulation. However, all fragments produced via collisional fragmentation cannot be treated individually by  $N$  body simulation because of computational limitation. Therefore, one applies the super-particle approximation where a super particle represents a large number of planetesimals and fragments. This method is applied for planet formation (Levison et al. 2012; Morishima 2015; Walsh, & Levison 2019) and for debris disks (Kral et al. 2013; Nesvold et al. 2013). In this paper, we newly develop the  $N$  body code including the mass evolution of planetesimals via collisional cascade, which allows us to evaluate dynamical friction and collisional fragmentation in the giant impact stage. In §. 2, we explain the method to develop the code. In §. 3, we conduct test calculations for the collisional cascade and validate the method. In §. 4, we perform simulations for the orbital evolution of protoplanets in planetesimal or giant-impact-ejecta disks using the newly developed code. In §. 5, we discuss the effect of remnant planetesimals and giant impact ejecta on the orbital evolution of protoplanets in the giant impact stage. We summarize our finding in §. 6.

## 2. METHOD

In the giant impact stage, the orbital evolution and collisions of protoplanets occur. The gravitational inter-

action with a planetesimal disk is important for the final orbits of protoplanets. However, the disk mass of planetesimals decreases due to the collisional cascade starting from planetesimal fragmentation. Therefore, we need to treat the evolution of orbits and masses consistently.

We apply the super-particle approximation for planetesimals and smaller bodies ejected by collisional fragmentation; a super particle represents to planetesimals and collisional fragments. Meanwhile, we apply a single particle for a single protoplanet. We numerically integrate the equations of motion of particles via the fourth order Hermite scheme (Makino, & Aarseth 1992; Kokubo, & Makino 2004). The orbital integration allows us to accurately treat dynamical evolution and direct collisions between protoplanets and super particles<sup>1</sup>. However, the number of super particles that we apply is much smaller than that of planetesimals and fragments with which we are concerned so that statistical treatment is required for accurate calculation of interactions between super particles.

Morishima (2015) developed a method for the collisions and dynamical interactions between super particles in  $N$ -body simulations. We treat the collisions between super particles following Morishima (2015), while we ignore the dynamical interaction because the collisional timescale is much shorter than the dynamical interaction timescale for dynamically hot planetesimals.

We consider the  $j$ -th super particle at the cylindrical coordinate  $(r_j, \theta_j, z_j)$  originated at the host star with mass  $M_*$ . The surface density around the super particle,  $\Sigma_j$ , is determined by the total mass of super particles in the area with  $r = [r_j - \delta r_j : r_j + \delta r_j]$  and  $\theta = [\theta_j - \delta \theta_j : \theta_j + \delta \theta_j]$ ;

$$\Sigma_j = \frac{1}{4r_j\delta r_j\delta \theta_j} \left[ m_j + \sum_k^{N_{n,j}} m_k \right], \quad (1)$$

where  $N_{n,j}$  is the number of super particles in the area and  $m_k$  is the mass of the  $k$ -th super particle in the area. We choose  $\delta r$  and  $\delta \theta$  according to the accuracy of mass evolution of planetesimals due to the collisional cascade, which we discuss in §3.

The relative velocity, which characterises collisional fragmentation of planetesimals in super particles, is determined by the orbital elements of super particles in the area. We calculate the relative velocity  $v_j$  between planetesimals in the  $j$ -th super particle with semimajor axis  $a_j$ , eccentricity  $e_j$ , inclination  $i_j$ , the longitude of pericenter  $\varpi_j$ , and the longitude of ascending node  $\Omega_j$ , given by

$$v_{r,j} = v_K \sqrt{e_{r,j}^2 + i_{r,j}^2}, \quad (2)$$

where  $v_K = \sqrt{GM_*/a_j}$ ,  $G$  is the gravitational constant, and

$$e_{r,j}^2 = \frac{1}{N_{n,j}} \sum_k^{N_{n,j}} [e_j^2 + e_k^2 - 2e_j e_k \cos(\varpi_j - \varpi_k)], \quad (3)$$

<sup>1</sup> The total ejecta mass caused by collisions between protoplanets and super particles is estimated to be much smaller than the disk mass and their collisional lifetimes are much shorter than that of the disk. Therefore, we ignore collisional ejecta caused by collisions between protoplanets and super particles.

$$i_{r,j}^2 = \frac{1}{N_{n,j}} \sum_k^{N_{n,j}} [i_j^2 + i_k^2 - 2i_j i_k \cos(\Omega_j - \Omega_k)]. \quad (4)$$

The collisional cascade grinds planetesimals down to micron-sized grains, which are blown out due to the radiation pressure of the host star (e.g., Kobayashi et al. 2008, 2009; Krivov 2010). Collisional fragmentation of planetesimals thus reduces the surface density of planetesimals due to the collisional cascade. We consider the quasi-steady-state collisional cascade, for which Kobayashi & Tanaka (2010) derived the reduction rate of the surface density of planetesimals, given by

$$\frac{d\Sigma}{dt} = -\frac{(2 - \alpha_c)^2}{m_c^{1/3}} \Sigma^2 \Omega_K \left( \frac{v_r(m_c)^2}{2Q_D^*(m_c)^*} \right)^{\alpha_c - 1} f(\alpha_c), \quad (5)$$

where  $m_c$  is the mass of largest bodies in the collisional cascade,  $\alpha_c$  is the index of the mass distribution of bodies determined by the collisional cascade,  $f(\alpha_c)$  is the dimensionless value dependent on  $\alpha_c$ , and  $Q_D^*$  is the specific impact energy needed for the ejection of the half mass of colliders. The mass of largest bodies  $m_c$  does not change in the collisional cascade, which is valid until the bodies with  $m_c$  exist. For  $v_r^2/Q_D^* \propto m^p$ ,  $\alpha_c$  is given by (Kobayashi & Tanaka 2010)

$$\alpha_c = \frac{11 + 3p}{6 + 3p}. \quad (6)$$

The mass distribution with the index  $\alpha_c$  is achieved in the timescale for the collisional cascade. An earlier mass distribution index may be different from  $\alpha_c$  in Eq. (6). However, the mass loss due to the collisional cascade is negligible in such an early stage and the mass evolution mainly occurs when the mass distribution given by Eq. (6) is achieved. Therefore, Eqs. (5) and (6) are valid to treat the surface density evolution accurately. According to Kobayashi & Tanaka (2010),  $f(\alpha_c)$  is given by

$$f(\alpha_c) = 1.055\rho^{-2/3} \left[ \left( -\ln \epsilon + \frac{1}{2-b} \right) s_1(\alpha_c) + s_2(\alpha_c) + s_3(\alpha_c) \right], \quad (7)$$

where  $\rho$  is the density of bodies,  $b$  is the power-law index of the mass distribution of fragments,  $\epsilon$  is the constant determining the largest mass of fragments, and<sup>2</sup>

$$s_1(\alpha_c) = \int_0^\infty d\phi \frac{\phi^{1-\alpha_c}}{1+\phi}, \quad (8)$$

$$s_2(\alpha_c) = - \int_0^\infty d\phi \frac{\phi^{1-\alpha_c}}{1+\phi} \ln \frac{\phi}{(1+\phi)^2}, \quad (9)$$

$$s_3(\alpha_c) = \int_0^\infty d\phi \frac{\phi^{-\alpha_c}}{1+\phi} \ln(1+\phi). \quad (10)$$

The impact laboratory experiments shows  $b = 1.5 - 1.7$  and  $\epsilon \sim 0.1$  (e.g., Takagi et al. 1984; Nakamura, & Fujiwara 1991) so that the choice of  $b$  and  $\epsilon$  insignificantly change the value of  $f(\alpha_c)$ .<sup>3</sup> Therefore, we set  $b = 3/5$

<sup>2</sup> We correct a typo in  $s_3(\alpha_c)$  of Kobayashi & Tanaka (2010).

<sup>3</sup> We here evaluate the dependence of  $f(\alpha_c)$  on  $b$ . We consider  $p = 0.453$ , and then  $\alpha_c = 1.68$ . The values of  $s_1$ ,  $s_2$ , and  $s_3$  are calculated to be 3.7, 7.4, and 2.6, respectively. The function  $f(1.68)$  with  $\epsilon = 0.2$  is estimated to be 28.9 and 33.8 for  $b = 1.5$  and 1.7, respectively.

and  $\epsilon = 0.2$ .

If  $v_r$  is fixed, the integration of Eq. (5) over time  $t$  gives

$$\Sigma(t) = \frac{\Sigma(0)}{1 + t/\tau_0}, \quad (11)$$

where  $\tau_0 = -\Sigma(0)/\dot{\Sigma}(0)$ . In the giant impact stage, Eq. (11) is not always valid because of the evolution of  $v_r$ . Therefore, we use Eq. (11) only for the validation of our simulation in §3.

Based on Eq. (5), the mass-loss rate of the  $j$ -th super particle due to the collisional cascade is given by

$$\frac{1}{m_j} \frac{dm_j}{dt} = -\frac{(2 - \alpha_c)^2}{m_{c,j}^{1/3}} \Sigma_j \Omega_K \left( \frac{v_{r,j}^2}{2Q_D(m_{c,j})^*} \right)^{\alpha_c - 1} f(\alpha_c), \quad (12)$$

where  $m_{c,j}$  is the mass of the largest bodies in the  $j$ -th super particle. We calculate the mass evolution of super particles via the integration of Eq. (12) using Eqs.(1) and (2).

The masses of the largest bodies in super particles,  $m_c$ , are set to  $\gtrsim 10^{16}$  g corresponding to  $\gtrsim 1$  km in radius. Therefore,  $Q_D^*$  of such a body is mainly determined by shuttering and gravitational reaccumulation (Benz & Asphaug 1999; Leinhardt, & Stewart 2012; Jutzi 2015; Genda et al. 2015, 2017; Suetsugu et al. 2018). Therefore,  $Q_D^*$  has a monotonous increasing function of  $m_c$ , which is assumed to be (e.g., Benz & Asphaug 1999)

$$Q_D^* = Q_0 \left( \frac{m_c}{10^{21} \text{ g}} \right)^p, \quad (13)$$

where  $Q_0$  and  $p$  are determined from numerical simulations. The collisional cascade is controlled not by individual collisions but by successive collisions. The value averaged over impact angles is applied for  $Q_D^*$ . Taking into account self-gravity and a model of rock fractures, Benz & Asphaug (1999) obtained the averaged values for  $Q_0$  and  $p$  via the smoothed particle hydrodynamics (SPH) simulation. Recently, the dependence of  $Q_D^*$  on the number of SPH particles is argued and the value of  $Q_D^*$  decreases 20% in the limit of high resolution simulation (Genda et al. 2015). However, the friction of damaged rock, which was not considered in Benz & Asphaug (1999), increases  $Q_D^*$  (Jutzi 2015). The value of  $Q_D^*$  obtained in Benz & Asphaug (1999) is similar to that given by the high-resolution simulations with the fraction (Suetsugu et al. 2018). Therefore, we set  $Q_0 = 9.5 \times 10^8 \text{ erg/g}$  and  $p = 0.453$  (Benz & Asphaug 1999).

### 3. VALIDATION FOR COLLISIONAL CASCADE

We perform a simulation for collisional evolution of a planetesimal disk composed of 2,000 super particles with  $a = 0.975\text{--}1.025$  AU and  $m_c = 10^{16}$  g. The radial distribution of super particles is put according to  $\Sigma(a) \propto a^{-1}$  and  $e$  and  $i$  have the Rayleigh distributions with mode values  $e = 0.01(a/1 \text{ AU})^{1/2}$  and  $i = 0.005(a/1 \text{ AU})^{1/2}$ . The collisional-cascade timescale in this setting is estimated to be  $\tau_0 \approx 0.6$  years. We evaluate the accuracy of the method from the comparison with the analytic solution in Eq. (11) at  $t = 100$  years.

The accuracy of the simulation depends on the number of particles in the neighbor area,  $N_n$ . We calculate the

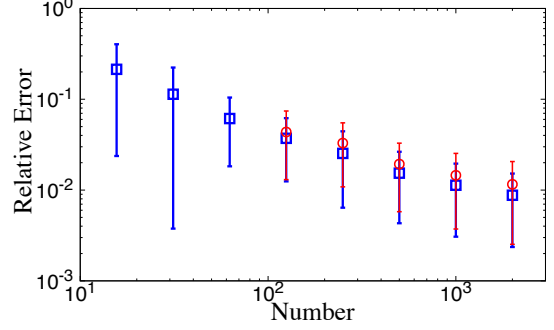


**Figure 1.** Relative errors of the surface density at  $t = 100$  years with the setting of  $\tau_0 \approx 0.6$  years for  $\delta\theta = \pi/8$  (red circles) and  $\pi$  (blue squares), as a function of the number of super particles. The error bars indicate the standard errors obtained from 40 runs.

relative error of the surface density from comparison of the simulation with the analytical solution. Fig. 3 shows the dependence of relative errors on the number of super particles. The errors are roughly proportional to the number of super particles, which is proportional to  $N_n$  for fixed  $\delta\theta$ . However, the errors are almost independent of  $\delta\theta$ . Although  $N_n$  decreases with decreasing  $\delta\theta$ , the number of particles having the experience in a neighbor area is almost same in the time much longer than orbital periods if the number of super particles and  $\delta r$  are fixed. The timescale of the collisional cascade is mainly much longer than orbital periods. Therefore, the accuracy better than 10% is obtained if the number of particles in the annulus with width  $\delta r$  is  $\gtrsim 10$ .

### 4. ORBITAL EVOLUTION OF PROTOPLANETS IN A SWARM OF FRAGMENTING PLANETESIMALS

We carry out simulations for the orbital evolution of 3 protoplanets with an Earth mass  $M_\oplus$  in a planetesimal disk with  $30M_\oplus$  composed of 3,000 super particles around the central star with solar mass  $M_\odot$ . The semi-major axis of the intermediate protoplanet is initially set at 1 AU, the orbital separation of protoplanets is 10 mutual Hill radii, and their eccentricities and inclinations are 0.03 and 0.015, respectively. The radial distribution of super particles is initially put according to  $\Sigma(a) \propto a^{-1}$  and their  $e$  and  $i$  have the Rayleigh distributions with mode values  $e = 0.03$  and  $i = 0.015$ , respectively. The intermediate radius and width of the planetesimal disk are 1 AU and 30 mutual Hill radii, respectively. For the treatment of collisional fragmentation, we put  $\delta r = 0.01$  AU and  $\delta\theta = \pi/8$ .

The collisional cascade is characterized by planetesimal mass  $m_c$ . We set  $m_c = 10^{16}$  g ( $\approx 1$  km in radius) for collisional fragmentation, while we have an additional simulation without collisional fragmentation ( $Q_D^* = \infty$  or  $m_c = \infty$ ). Figure 4a,b shows the orbital distribution of protoplanets and super particles at  $t = 10^3$  years with collisional fragmentation, while Figure 4c,d is that without fragmentation. Dynamical friction decreases  $e$  and  $i$  of protoplanets, while  $e$  and  $i$  of planetesimals increase. Increases in  $e$  and  $i$  of planetesimals activate their collisional cascade, which reduces the surface density of planetesimals. Collisional fragmentation weakens dynamical friction so that  $e$  and  $i$  of protoplanets with fragmentation remain higher than those without fragmentation.

Figures 4–4 show the evolution of the root mean squares of eccentricities  $\langle e^2 \rangle^{1/2}$  and inclinations  $\langle i^2 \rangle^{1/2}$

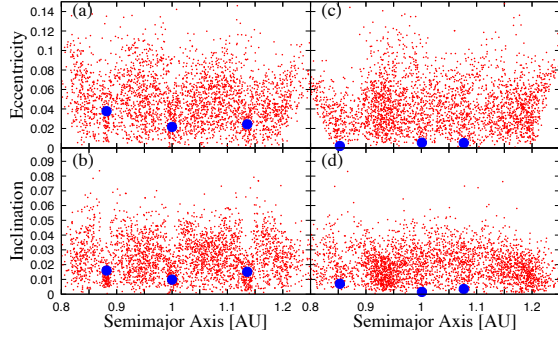


**Figure 2.** Eccentricities (a,c) and inclinations in radian (b,d) of super particles (red dots) and protoplanets (blue filled circles) with fragmentation (a,b) or without fragmentation (c,d).

for planetesimals and protoplanets in the same initial setting of planetesimal disks and protoplanets as Figure 4. If we ignore collisional fragmentation,  $\langle e^2 \rangle^{1/2}$  and  $\langle i^2 \rangle^{1/2}$  of planetesimals become much larger than those of protoplanets (Figure 4). This is caused by dynamical friction. However, collisional fragmentation of planetesimals decreases the surface density of planetesimals (Figures. 4 and 4), which suppresses the  $e$  and  $i$  reduction of protoplanets via dynamical friction. Collisional fragmentation is effective for small  $m_c$  so that  $\langle e^2 \rangle^{1/2}$  and  $\langle i^2 \rangle^{1/2}$  of protoplanets insignificantly change. On the other hand, the  $e$  and  $i$  evolution for planetesimals are almost independent of fragmentation. This is because the viscous stirring of protoplanets controls  $e$  and  $i$  of planetesimals.

If we consider two populations of bodies such as protoplanets with  $\langle e^2 \rangle_1^{1/2}$ ,  $\langle i^2 \rangle_1^{1/2}$ , and mass  $m_{p,1}$  and planetesimals with  $\langle e^2 \rangle_2^{1/2}$ ,  $\langle i^2 \rangle_2^{1/2}$ , and mass  $m_{p,2}$ , the time differential of  $\langle e^2 \rangle_\alpha^{1/2}$  and  $\langle i^2 \rangle_\alpha^{1/2}$  for  $\alpha = 1$  or  $2$  (protoplanets or planetesimals) due to dynamical friction and viscous stirring is analytically given by (Ohtsuki et al. 2002)

$$\frac{d\langle e^2 \rangle_\alpha}{dt} = a_0^2 \Omega \sum_{\beta=1,2} \left[ N_{s,\beta} \frac{h_{\alpha,\beta}^4 m_{p,\beta}}{(m_{p,\alpha} + m_{p,\beta})^2} \left( m_{p,\beta} P_{VS} + \frac{m_{p,\beta} \langle e^2 \rangle_\beta - m_{p,\alpha} \langle e^2 \rangle_\alpha}{\langle e^2 \rangle_\alpha + \langle e^2 \rangle_\beta} P_{DF} \right) \right], \quad (14)$$

$$\frac{d\langle i^2 \rangle_\alpha}{dt} = a_0^2 \Omega \sum_{\beta=1,2} \left[ N_{s,\beta} \frac{h_{\alpha,\beta}^4 m_\beta}{(m_{p,\alpha} + m_{p,\beta})^2} \left( m_{p,\beta} Q_{VS} + \frac{m_{p,\beta} \langle i^2 \rangle_\beta - m_{p,\alpha} \langle i^2 \rangle_\alpha}{\langle i^2 \rangle_\alpha + \langle i^2 \rangle_\beta} Q_{DF} \right) \right], \quad (15)$$

where  $a_0$  is the mean semimajor axis of bodies,  $N_{s,\beta}$  is the surface number density of bodies for  $\beta = 1$  or  $2$ ,  $h_{\alpha,\beta} = [(m_{p,\alpha} + m_{p,\beta})/3M_*]^{1/3}$  is the reduced Hill radius of bodies with masses  $m_{p,\alpha}$  and  $m_{p,\beta}$ ,  $P_{VS}$ ,  $P_{DF}$ ,  $Q_{VS}$ , and  $Q_{DF}$  are the efficiencies for viscous stirring and dynamical friction for  $\langle e^2 \rangle_{1,2}$  and  $\langle i^2 \rangle_{1,2}$ , respectively. The analytical formulae of  $P_{VS}$ ,  $P_{DF}$ ,  $Q_{VS}$ , and  $Q_{DF}$  are given as a function of  $\langle e^2 \rangle_{1,2}$  and  $\langle i^2 \rangle_{1,2}$  in Ohtsuki et al. (2002).

The  $e$  and  $i$  variation rates due to dynamical friction are given by the second terms on the right hand sides of Eqs. (14) and (15), respectively. Protoplanets are much more massive than planetesimals ( $m_{p,1} \gg m_{p,2}$ ). For  $m_{p,1} \langle e^2 \rangle_1 \gg m_{p,2} \langle e^2 \rangle_2$  and  $m_{p,1} \langle i^2 \rangle_1 \gg m_{p,2} \langle i^2 \rangle_2$ ,

the dynamical-friction damping rates for protoplanets is approximated to be

$$\frac{1}{P_{DF}} \frac{d\langle e^2 \rangle_1}{dt} \sim \frac{1}{Q_{DF}} \frac{d\langle i^2 \rangle_1}{dt} \sim -\frac{a_0^2 \Omega \Sigma}{6M_*} \left( \frac{m_{p,1}}{3M_*} \right)^{1/3}, \quad (16)$$

where  $\Sigma$  is the surface density of planetesimals and we assume  $\langle e^2 \rangle_1 \approx \langle e^2 \rangle_2$  and  $\langle i^2 \rangle_1 \approx \langle i^2 \rangle_2$ . The damping rates are mainly determined by  $\Sigma$  but are almost independent of the choice of planetesimal masses,  $m_{p,2}$ . This means the super-particle approximation is valid. However, dynamical friction leads to the equipartition of the random energies such as  $m_{p,1} \langle e^2 \rangle_1^{1/2} \sim m_{p,2} \langle e^2 \rangle_2^{1/2}$  and  $m_{p,1} \langle i^2 \rangle_1^{1/2} \sim m_{p,2} \langle i^2 \rangle_2^{1/2}$ . The values for the equipartition depend on the choice of  $m_{p,2}$ . Therefore, we need to care the choice of super-particle masses if we are interested in the equipartition.

To compare the results of simulations with Eqs. (14) and (15), we set  $m_{p,2}$  to be super-particle mass  $m_j$  and integrate Eqs. (14) and (15) over time (see Fig. 4). The analytic solution is consistent with the simulation. For  $t \gtrsim 100$  years, dynamical friction is ineffective because of the achievement of energy equipartition such as  $m_{p,1} \langle e^2 \rangle_1^{1/2} \sim m_{p,2} \langle e^2 \rangle_2^{1/2}$  and  $m_{p,1} \langle i^2 \rangle_1^{1/2} \sim m_{p,2} \langle i^2 \rangle_2^{1/2}$ . The result depends on the super-particle mass as discussed above. However, collisional fragmentation mainly occur prior to the achievement of the equipartition (see Figs. 4 and 4).

The mass of planetesimals  $m_{p,2}$  in Eqs. (14) and (15) is initially set to be super-particle masses  $m_j$ , although  $m_c$  in Eq. (5) is independently given. We then integrate Eqs. (5), (14), and (15) over time. The analytic solution is roughly in agreement with the results of simulations (see Figs. 4 and 4). In the simulations, each super particle has an independent mass. Super particles in the inner disk effectively lose their masses via collisional fragmentation because of high collisional speeds, while super particles tend to have large masses in the outer disk. On the other hand, the mass evolution of planetesimal disks is calculated with the averaged collisional speed in the analytical solution. Therefore, the analytic solution cannot perfectly reproduce the simulations. However, the tendency of orbital interaction and collisional fragmentation is understood from the analytical solution.

It should be noted that the relative increases in protoplanet masses are smaller than 0.2 and 0.02 in the case without and with collisional fragmentation, respectively. Those are caused by collisions with planetesimals. We estimate the effect of collisional damping due to the collisional accretion according to the model by Kobayashi et al. (2016), resulting in the  $e$  damping of 0.006 and 0.0001 for protoplanets without and with collisional fragmentation, respectively. The collisional damping insignificantly affects the orbital evolution of protoplanets. Therefore, the analytical solution without collisional damping is in good agreement with the results of simulations.

The timescale of dynamical friction is estimated from Eqs. (14) and (15). If  $m_{p,1} \langle e^2 \rangle_1^{1/2} \gg m_{p,2} \langle e^2 \rangle_2^{1/2}$  and  $\langle e^2 \rangle_2^{1/2} \gg \langle e^2 \rangle_1^{1/2}$  for  $m_{p,1} \gg m_{p,2}$ , the  $\langle e^2 \rangle_1^{1/2}$  damping timescale due to dynamical friction has the relation as

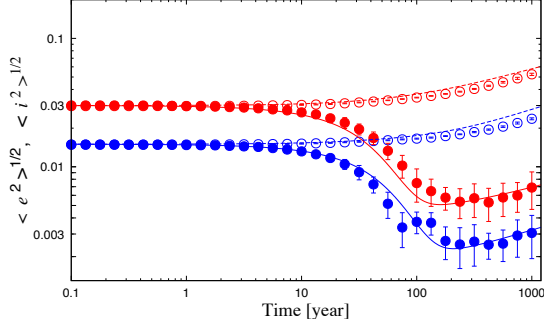


**Figure 3.** The root mean squares of eccentricities  $\langle e^2 \rangle^{1/2}$  (red) and inclinations  $\langle i^2 \rangle^{1/2}$  (blue) for planetesimals (open circles) and protoplanets (filled circles) without collisional fragmentation in the planetesimal disk same as Fig. 4. The error bars are given by the standard deviation of 13 runs. Analytic solutions  $\langle e^2 \rangle^{1/2}$  and  $\langle i^2 \rangle^{1/2}$  for planetesimals (dotted lines) and protoplanets (solid lines) is obtained from the time integration of Eqs. (14) and (15).

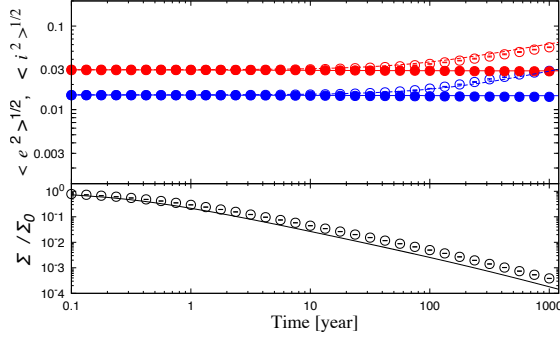


**Figure 4.** Same as Fig. 4 but for the treatment of collisional fragmentation. We take into account collisional fragmentation for  $m_c = 1 \times 10^{16}$  g. The mean surface density of planetesimals,  $\Sigma$ , decreases due to collisional fragmentation. The ratio of  $\Sigma$  to initial surface density  $\Sigma_0$  obtained from the simulation (open circles) and the analytical solution (solid line) is shown in the bottom panel.

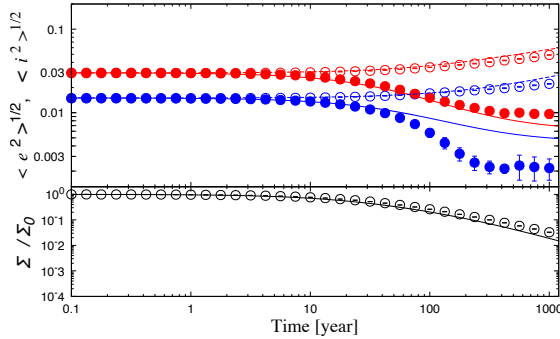


**Figure 5.** Same as Fig. 4 but for  $m_c = 1 \times 10^{19}$  g. (Ohtsuki et al. 2002)

$$\tau_{\text{df}} \approx 1 \times 10^4 \left( \frac{M_{\text{disk}}}{M_{\oplus}} \right)^{-1} \left( \frac{\langle e^2 \rangle_2^{1/2}}{0.1} \right)^2 \left( \frac{P_{\text{DF}}}{17} \right)^{-1} \times \left( \frac{\Delta a}{10 r_{\text{H}}} \right) \left( \frac{a_0}{1 \text{ AU}} \right)^{3/2} \left( \frac{M_*}{M_{\odot}} \right)^{1/2} \text{ yr}, \quad (17)$$

where  $M_{\text{disk}}$  is the total mass of a planetesimal disk,  $\Delta a$  is the width of the disk, and  $r_{\text{H}} = (m_{\text{p},1}/3M_*)^{1/3} a_0$  is the Hill radius for protoplanets. Note that  $P_{\text{DF}}$  is estimated to be  $\sim 10$  for  $m_{\text{p},1} \sim M_{\oplus}$  and  $\langle e^2 \rangle_1^{1/2} \approx \langle e^2 \rangle_2^{1/2} \sim 0.1$ .

This estimate implies a planetesimal disk with  $M_{\text{disk}} \ll M_{\oplus}$  leads to eccentricity damping for Earth-sized protoplanets in a long timescale  $\gg 10^4$  yr via dynamical friction. In addition, dynamical friction increases  $\langle e^2 \rangle^{1/2}$  of planetesimals. The increase in  $\langle e^2 \rangle_2^{1/2}$  makes  $\tau_{\text{df}}$  longer.

On the other hand, the decreasing timescale for  $M_{\text{disk}}$  due to the collisional cascade,  $\tau_{\text{cc}}$ , is estimated from Eq. (5) to be (Kobayashi & Tanaka 2010)

$$\tau_{\text{cc}} \approx 4 \times 10^3 \left( \frac{M_{\text{disk}}}{M_{\oplus}} \right)^{-1} \left( \frac{\langle e^2 \rangle_2^{1/2}}{0.1} \right)^{-1.36} \left( \frac{Q_0}{9.5 \times 10^8 \text{ erg/g}} \right)^{0.68} \times \left( \frac{m_c}{10^{22} \text{ g}} \right)^{0.79} \left( \frac{\Delta a}{0.1 a_0} \right) \left( \frac{a_0}{1 \text{ AU}} \right)^{4.18} \text{ yr}. \quad (18)$$

For 100 km-sized planetesimals ( $m_c \approx 10^{22}$  g) with  $\langle e^2 \rangle_2^{1/2} \sim 0.1$ ,  $\tau_{\text{cc}} \lesssim \tau_{\text{df}}$ . It should be noted that dynamical friction increases  $\langle e^2 \rangle_2^{1/2}$  during the  $\langle e^2 \rangle_1^{1/2}$  damping, which shortens  $\tau_{\text{cc}}$  and elongates  $\tau_{\text{df}}$  as discussed above. Therefore, even if  $\tau_{\text{cc}} \sim \tau_{\text{df}}$  initially,  $\tau_{\text{cc}}$  eventually becomes much shorter than  $\tau_{\text{df}}$ .

Equations (17) and (18) show  $\tau_{\text{df}}/\tau_{\text{cc}}$  is independent of  $M_{\text{disk}}$  and  $\Delta a$  but depends on  $\langle e^2 \rangle_1^{1/2}$ ,  $\langle e^2 \rangle_2^{1/2}$ , and  $m_c$ . For  $\langle e^2 \rangle_1^{1/2} = \langle e^2 \rangle_2^{1/2} = 0.03$ ,  $P_{\text{DF}} \approx 60$  so that  $\tau_{\text{cc}} \ll \tau_{\text{df}}$  for  $m_c = 10^{16}$  g, while  $\tau_{\text{df}} \sim \tau_{\text{cc}}$  for  $m_c \sim 10^{19}$  g. Therefore, as shown in Figs. 4 and 5,  $e$  and  $i$  of protoplanets insignificantly decrease for  $m_c = 10^{16}$  g because of  $\tau_{\text{cc}} \ll \tau_{\text{df}}$ , while those are moderately damped for  $\tau_{\text{cc}} \sim \tau_{\text{df}}$  with  $m_c = 10^{19}$  g. Therefore, the condition with  $t_{\text{cc}} \gg \tau_{\text{df}}$  is required for the  $e$  damping of protoplanets.

Planets formed via giant impacts have high eccentricities and inclinations. For Earth-sized planets formed in the giant impact stages, the mean eccentricity is  $\sim 0.1$  (Chambers 2001; Kokubo et al. 2006), which is much larger than the current eccentricities of Earth and Venus. The depletion timescale of a planetesimal disk with  $m_c \lesssim 10^{21}$  g is shorter than the  $e$  damping timescale via dynamical friction (see Eqs. 17 and 18). Therefore, larger planetesimals are required for  $e$  damping of Earth-sized planets. We consider such large planetesimals are produced from a giant impact. The mass ratios of largest giant impact ejecta to parent protoplanets are  $\sim 0.01$  (Genda et al. 2015). Therefore, we consider  $m_c \sim 10^{26}$  g, resulting in  $\tau_{\text{cc}} \gg \tau_{\text{df}}$ .

We perform the simulation for the orbital evolution of a high-eccentricity planet with mass  $M_{\oplus}$  in a swarm of giant impact ejecta. Giant impact ejecta initially have similar orbits to parent planets. However,  $\varpi$  and  $\Omega$  are eventually distributed uniformly due to perturbation from other planets. The timescale to achieve a uniform distribution for  $\varpi$  and  $\Omega$ , which is roughly given by the precession rates for  $\varpi$  and  $\Omega$  obtained from the secular perturbation theory (Murray, & Dermott 1999), is estimated as  $\sim 10^5 - 10^6$  years for giant impact ejecta around 1 AU perturbed by a Venus-like planet, which is much shorter than the timescale for dynamical friction caused by giant impact ejecta. Therefore, instead of ignoring perturbation from other planets, we uniformly set  $\varpi$  and  $\Omega$  of giant impact ejecta from the beginning. We initially set  $a = 1 \text{ AU}$  and  $e = 2i = 0.1$  for the planet and  $a = 0.95 -$



1.05 AU and  $\langle e^2 \rangle^{1/2} = 2\langle i^2 \rangle^{1/2} = 0.1$  for a giant-impact-ejecta disk composed of 120 super particles with total mass  $0.2M_\oplus$  and  $m_c = 10^{26}$  g (Fig. 4). The evolutions of  $\langle e^2 \rangle^{1/2}$  and  $\langle i^2 \rangle^{1/2}$  for giant impact ejecta and the planet differs from those predicted by the analytical solutions given by the time integration of Eqs. (5), (14), and (15). Once  $\langle e^2 \rangle^{1/2}$  and/or  $\langle i^2 \rangle^{1/2}$  are much larger than 0.1, their orbits are controlled by the higher order terms for  $\langle e^2 \rangle^{1/2}$  and  $\langle i^2 \rangle^{1/2}$ , which are ignored in Eqs.(14) and (15). The higher order terms make dynamical friction less effective. Therefore, the variations of  $\langle e^2 \rangle^{1/2}$  and  $\langle i^2 \rangle^{1/2}$  for the planet and planetesimals are less than those expected by the analytic solution. However,  $e$  of the planet becomes comparable to or larger than the analytic estimate until 10 Myrs and decreases much greater than the analytic estimate in several 10 Myrs. This is caused by the orbital energy damping for the planet rather than its angular momentum variation. If the angular momentum is fixed, the energy damping given by  $-\Delta a/a$  results in  $\Delta e = (1 - e^2)\Delta a/2ae$ , where  $\Delta e$  and  $\Delta a$  are the changes in  $e$  and  $a$ , respectively. Therefore, even a small energy damping of  $\Delta a/a \approx -0.02$  leads to  $\Delta e \approx -0.1$  for the planet. Giant impact ejecta are scattered by the planet and tend to stay in the outer disk so that the planet loses the orbital energy via the scatterings. This is clearly shown in the semimajor-axis evolution for the planet and giant impact ejecta (Fig. 4). The collisional damping between the planet and giant impact ejecta also reduces the orbital energy of the planet. The accretion mass of giant impact ejecta onto the planet is  $0.086_{-0.006}^{+0.004}M_\oplus$  in 10 Myrs,  $0.029_{-0.005}^{+0.011}M_\oplus$  for  $t = 10$ –30 Myrs, and  $0.029_{-0.004}^{+0.04}M_\oplus$  for  $t = 30$ –100 Myrs. Although the  $e$  damping is significant after 30 Myrs, the collisional damping expected from the accretion mass is slight. Therefore, the energy loss for the planet due to the scattering of giant impact ejecta mainly decreases its eccentricity.

The mass evolution of giant impact ejecta due to collisional fragmentation is less important than that estimated by Eq. (5). Increase in  $e$  of giant impact ejecta due to planetary perturbation makes the giant-impact-ejecta disk wider. This decreases the surface density of giant impact ejecta, which reduces the efficiency of collisional fragmentation. In addition, collisions between high-eccentricity giant impact ejecta are more frequent around the planetary orbit. Collisional fragmentation between giant impact ejecta with similar  $\varpi$  and  $\Omega$  thus mainly occurs so that those relative velocities are comparatively small (see Eqs. 3 and 4). The mass loss by collisional fragmentation is thus less effective due to the increase of ejecta eccentricity. Therefore, the giant-impact-ejecta disk is maintained in a long timescale  $\gtrsim 10$  Myr, resulting in the significant eccentricity damping for the planet.

## 5. DISCUSSION

In the giant impact stage, orbital instability of protoplanets occurs in a timescale longer than 10 Myrs (Chambers et al. 1996; Chambers, & Wetherill 1998; Iwasaki et al. 2001, 2002; Kominami, & Ida 2002; Kokubo et al. 2006). The protoplanets formed from the long-term evolution mainly have high eccentricities ( $\sim 0.1$ ) (Chambers 2001; Kokubo et al. 2006), which are much larger than

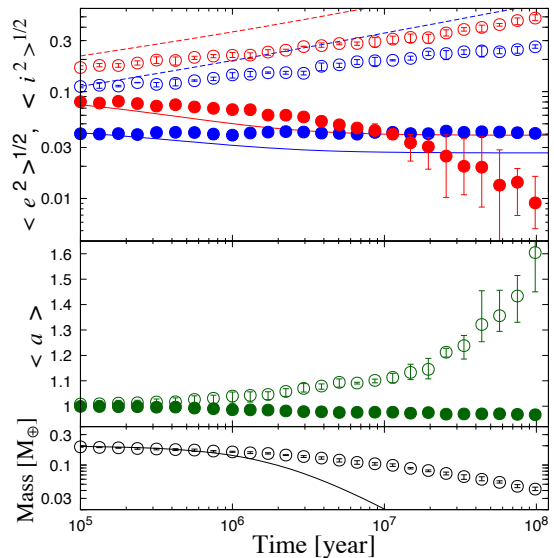


**Figure 6.** The orbital and mass evolution of a planet and a swarm of giant impact ejecta. Top panel shows  $\langle e^2 \rangle^{1/2}$  (red) and  $\langle i^2 \rangle^{1/2}$  (blue) for the protoplanet (filled circles) and giant impact ejecta (open circles). Middle panel also shows  $\langle a \rangle$  (green). Bottom panel represents the total mass of giant impact ejecta. We carry out three runs with different initial positions. The error bars indicate the minimum and maximum values. The lines are the same as Fig. 4.

the current eccentricities of Earth and Venus. A swarm of planetesimals may damp the eccentricities of protoplanets due to dynamical friction (O’Brien et al. 2006; Raymond et al. 2009; Morishima et al. 2010). Instead, dynamical friction increases eccentricities of planetesimals, which induces collisional fragmentation between planetesimals. The collisional cascade grinds planetesimals until small fragments are brown out by radiation pressure, which results in the mass loss of the planetesimal disk. Collisional fragmentation may thus suppress the eccentricity damping for protoplanets. Therefore, we have investigated the orbital interaction between protoplanets and planetesimals, taking into account collisional fragmentation.

Eccentricities and inclinations of protoplanets are damped via dynamical friction if we ignore collisional fragmentation (see Fig. 4cd). However, collisional fragmentation weakens dynamical friction (see Fig. 4ab). The mass loss due to collisional fragmentation depends on the typical planetesimal size of which planetesimals mainly determine the total mass of the planetesimal disk. Collisional depletion occurs in a short timescale for planetesimal disks with small typical planetesimal sizes. For 100km-sized or smaller planetesimals, the eccentricity damping is ineffective due to collisional fragmentation (Figs. 4 and 4).

The primordial planetesimals may remain even in the giant impact stage. Although the typical size of primordial planetesimals is not unknown, the size may be on the order of 100 km, similar to that of Main-Belt asteroids (e.g., Kobayashi et al. 2016). Due to collisional fragmentation, dynamical friction for eccentricity damping is ineffective in such a planetesimal disk. On the other hand, the increase in the eccentricities of protoplanets is required for the onset of the orbital instability of protoplanets for giant impacts (Iwasaki et al. 2001). Although

primordial planetesimal disks may not explain the small eccentricities of Earth and Venus, such a disk does not inhibit the onset and maintain of giant impact stages (Walsh, & Levison 2019). In addition, the direct formation of Earth and Venus via the accretion of planetesimals is insignificant due to the depletion of remnant planetesimal disks via collisional fragmentation (Kobayashi et al. 2010; Kobayashi & Dauphas 2013). Therefore, collisional fragmentation supports the giant impact scenario to form Venus and Earth.

Giant impacts lead to the ejection of fragments as well as collisional growth of protoplanets. The collisional ejecta from single impacts have  $0.1\text{--}0.3M_{\oplus}$ , while the typical size of giant impact ejecta can be as large as 1,000 km (Genda et al. 2015). The simulation for the interaction between a protoplanet and giant impact ejecta shows significant eccentricity damping of the protoplanet in  $\gtrsim 30$  Myr (see Fig. 4). The collisional fragmentation is less effective in an originally narrow planetesimal disk for high-eccentricity planetesimals, while the dynamical friction is also less effective for high eccentricities and inclinations of planetesimals. As a result, eccentricity damping for planets occurs in a long timescale  $\sim 100$  Myr.

Giant impact ejecta are produced even in the early giant impact stage (Genda et al. 2015). However, the orbital separations of protoplanets are so narrow that giant impact ejecta are distributed widely due to interactions with other protoplanets. In addition, the eccentricity damping timescale due to dynamical friction is much longer than collisional timescale between protoplanets. Therefore, sequent giant impacts occurs due to insignificance of dynamical friction by giant impact ejecta. On the other hand, stable orbital configurations of protoplanets are achieved after tens of giant impacts. Such orbital separations are wide enough to keep the orbital concentration of giant impact ejecta around the orbits of single protoplanets. Therefore, dynamical friction by giant impact fragments is effective in the late giant impact stage, which may form low-eccentricity planets.

Finally we need to discuss the accuracy of the mass loss due to collisional fragmentation. As we discuss above, the collisional mass loss mainly occurs after the collisional cascade is achieved. In the collisional cascade, the mass loss is mainly determined by the total ejecta mass from single collisions, and is insensitive to the mass distribution of ejecta (Kobayashi & Tanaka 2010). Therefore, the uncertainty of collisional fragmentation mainly comes from  $Q_D^*$  at the typical sizes of planetesimals (see Eq. 18). As discussed in the previous studies (Kobayashi et al. 2016; Kobayashi, & Tanaka 2018),  $Q_D^*$  of 10 km-sized or smaller primordial planetesimals may be much larger than  $Q_D^*$  we set in the simulations. However, taking into account the enhancement of  $Q_D^*$ , 100 km-sized or smaller primordial planetesimals insignificantly work for the  $e$  damping of protoplanets. On the other hand,  $Q_D^*$  of 1000 km-sized bodies are mainly determined by the self-gravity of colliding bodies (Kobayashi et al. 2010, 2011; Genda et al. 2015, 2017; Suetsugu et al. 2018). The uncertainty is small for  $Q_D^*$  of largest ejecta of giant impacts. Therefore, the  $e$  damping of planets formed in the giant impact stage is likely to be caused by giant impact ejecta.

## 6. SUMMARY

Terrestrial planets are formed via giant impacts between Mars-sized protoplanets. The resultant planets have larger eccentricities than the current values for Earth and Venus. Dynamical friction with a planetesimal disk is expected to damp the eccentricities of protoplanets. On the other hand, the collisional cascade of planetesimals and blow-out of small collisional fragments by radiation pressure decrease the planetesimal disk mass, which weakens dynamical friction with planetesimals. Therefore, we have investigated the orbital evolution of planets with collisional fragmentation. Our findings are as follows.

1. We have developed an N-body simulation code involving the mass loss due to the collisional cascade. We have calculated the mass evolution of a planetesimal disk composed of super particles using the code, which reproduces the analytical solution for the mass loss due to the collisional cascade with high accuracy.
2. We have investigated the evolution of orbits and masses of protoplanets and planetesimals via gravitational interaction and collisional fragmentation using the N-body code. If collisional fragmentation is ignored, dynamical friction damps eccentricities and inclinations for protoplanets. However, collisional fragmentation suppresses dynamical friction. The timescale ratio of dynamical friction to collisional fragmentation depends on the typical planetesimal size but not on the disk mass. Even a massive planetesimal disk composed of 100km-sized or smaller planetesimals cannot damp eccentricities of planets. Therefore, the disks composed of primordial planetesimals are ineffective for the eccentricity damping for planets.
3. Giant impacts eject collisional fragments. The total masses of giant impact ejecta are several tenth of colliding planets. The typical size of the largest ejecta is  $\sim 1000$  km. We have carried out simulations for a planet with an Earth mass in the disk with 0.2 Earth masses composed of giant impact ejecta with largest ejecta  $10^{26}$  g. Collisional mass loss is insignificant for such a large typical size. Eccentricity of the planet is damped from 0.1 to  $\sim 0.01$  due to interactions with giant impact ejecta in  $\gtrsim 30$  Myrs. Therefore, giant impact ejecta are possible to decrease the eccentricities of planets formed via giant impacts, comparable to those of Earth and Venus.

We thank the reviewer for beneficial comments. The work is supported by Grants-in-Aid for Scientific Research (17K05632, 17H01105, 17H01103, 18H05436, 18H05438) from MEXT of Japan and by JSPS Core-to-Core Program “International Network of Planetary Sciences”.

## REFERENCES

- Benz, W., & Asphaug, E. 1999, *Icarus*, 142, 5  
 Chambers, J. E. 2001, *Icarus*, 152, 205  
 Chambers, J. E., & Wetherill, G. W. 1998, *Icarus*, 136, 304  
 Chambers, J. E., Wetherill, G. W., & Boss, A. P. 1996, *Icarus*, 119, 261

- Genda, H., Kobayashi, H., & Kokubo, E. 2015, *ApJ*, 810, 136
- Genda, H., Fujita, T., Kobayashi, H., et al. 2015, *Icarus*, 262, 58
- Genda, H., Fujita, T., Kobayashi, H., et al. 2017, *Icarus*, 294, 234
- Iwasaki, K., Emori, H., Nakazawa, K., et al. 2002, *PASJ*, 54, 471
- Iwasaki, K., Tanaka, H., Nakazawa, K., et al. 2001, *PASJ*, 53, 321
- Jutzi, M. 2015, *Planet. Space Sci.*, 107, 3
- Kobayashi, H., & Dauphas, N. 2013, *Icarus*, 225, 122
- Kobayashi, H., & Löhne, T. 2014, *MNRAS*, 442, 3266
- Kobayashi, H., & Tanaka, H. 2010, *Icarus*, 206, 735
- Kobayashi, H., Tanaka, H., Krivov, A. V., & Inaba, S. 2010, *Icarus*, 209, 836
- Kobayashi, H., Tanaka, H., & Krivov, A. V. 2011, *ApJ*, 738, 35
- Kobayashi, H., & Tanaka, H. 2018, *ApJ*, 862, 127
- Kobayashi, H., Tanaka, H., & Okuzumi, S. 2016, *ApJ*, 817, 105
- Kobayashi, H., Watanabe, S.-. ichiro ., Kimura, H., et al. 2008, *Icarus*, 195, 871
- Kobayashi, H., Watanabe, S.-. ichiro ., Kimura, H., et al. 2009, *Icarus*, 201, 395
- Kokubo, E., & Makino, J. 2004, *PASJ*, 56, 861
- Kokubo, E., Kominami, J., & Ida, S. 2006, *ApJ*, 642, 1131
- Kominami, J., & Ida, S. 2002, *Icarus*, 157, 43
- Kral, Q., Thébault, P., & Charnoz, S. 2013, *A&A*, 558, A121
- Krivov, A. V. 2010, *Research in Astronomy and Astrophysics*, 10, 383
- Levison, H. F., Duncan, M. J., & Thommes, E. 2012, *AJ*, 144, 119
- Leinhardt, Z. M., & Stewart, S. T. 2012, *ApJ*, 745, 79
- Makino, J., & Aarseth, S. J. 1992, *PASJ*, 44, 141
- Morishima, R. 2015, *Icarus*, 260, 368
- Morishima, R., Stadel, J., & Moore, B. 2010, *Icarus*, 207, 517
- Morishima, R. 2017, *Icarus*, 281, 459
- Murray, C. D., & Dermott, S. F. 1999, *Solar system dynamics* by C.D. Murray and S.F. McDermott. (Cambridge)
- Nakamura, A., & Fujiwara, A. 1991, *Icarus*, 92, 132
- Nesvold, E. R., Kuchner, M. J., Rein, H., et al. 2013, *ApJ*, 777, 144
- O'Brien, D. P., Morbidelli, A., & Levison, H. F. 2006, *Icarus*, 184, 39
- Ohtsuki, K., Stewart, G. R., & Ida, S. 2002, *Icarus*, 155, 436
- Raymond, S. N., O'Brien, D. P., Morbidelli, A., et al. 2009, *Icarus*, 203, 644
- Suetsugu, R., Tanaka, H., Kobayashi, H., et al. 2018, *Icarus*, 314, 121
- Takagi, Y., Mizutani, H., & Kawakami, S.-I. 1984, *Icarus*, 59, 462
- Walsh, K. J., & Levison, H. F. 2019, *Icarus*, 329, 88